

Control of Bypass Transitional Flow Past an Aerofoil by Plasma Actuation

Tapan K. Sengupta¹, V. K. Suman* and Yogesh G. Bhumkar

Department of Aerospace Engineering, Indian Institute of Technology Kanpur, Kanpur
208016, India

*National Aerospace Laboratory, Bangalore, India

ABSTRACT

In this work, we have studied effects of plasma actuation while controlling bypass transition of flow over the top surface of DU96-W-180 aerofoil. We have discussed some of the important plasma simulation models proposed in the literature and presented results using a hybrid model given by [Lemire and Vo, *J. Turbomach.*, 2011, 133(1), 011017]. Results show that the computed body force is localized near the electrodes. Due to action of plasma generated body force, bypass transition on the aerofoil surface is delayed.

Key words: Flow Control, Plasma Actuation, Direct Numerical Simulation, Bypass Transition, Transition Delay

1. INTRODUCTION

Control of flow is natural for an engineering device in order to simplify the design and operation, thereby increase the efficiency of the design. An aerofoil as a quintessential device provides the necessary lift, while experiencing least amount of resistance. Thus, the control of flow past an aerofoil would entail simultaneous increase of lift and reduction of drag. The shape has been termed streamlined due to high values of lift/drag ratio attained by such sections. Continual effort persists to reduce drag by keeping the flow laminar as far downstream as possible, without suffering transition to turbulence. This is due to the fact that flow turbulence leads to drag increase by an order of magnitude for streamlined bodies. For an aerofoil there can be many performance optimization goals, here we will confine our attention solely on transition delay.

Fluid flow transition can take place via multiple routes. A recent and up-to-date account of the subject is treated in [1]. A classical route of flow transition is attributed to evolution of viscous tuned waves, called as Tollmien-Schlichting (TS) waves. While there are instances where this mechanism is not present and researchers have looked for alternative routes, it was Morkovin [2] who coined the term bypass transition to indicate such routes. A detailed account of bypass transition can be found in [1, 3, 4] and many other references contained therein.

In recent times, significant progress have been made in magneto- and electro-hydrodynamic flow controls. Body forces arising as Lorentz forces help mitigate conditions which lead to transition and flow separation. Plasma actuators have been employed and their operating principles have been studied for a wide range of flows. First such published effort for transition delay is due to Velkoff and Ketcham [5] and a more recent overview of plasma flow control is given in Corke and Post [6]. Subsequently, plasma control has been utilized for lift augmentation of aerofoils by Corke and his co-authors [7, 8]; turbine blade separation control [9, 10]; bluff body flow control [11, 12]; separation delay [13, 14]; control of vortical flows [15]; high lift devices [16, 17] and noise control [18]. Plasma actuators hold promise due to lesser complications of construction and operation, having no moving parts, high bandwidth quick response, while adding lesser weight without creating noise and vibration.

Use of plasma actuator for turbulent drag reduction has been reported in [19]. Efforts at controlling flow transition caused by TS waves have been experimentally investigated in [20, 21]. Computational

¹Corresponding author; Phone no. +91 512 2597945; e-mail: tksen@iitk.ac.in (Tapan K. Sengupta).

efforts utilizing unsteady Navier-Stokes equation with appropriate plasma models have been reported in [22–28]. In these efforts, models are used for the electrodynamic field of the plasma.

One of the first model developed was by Massines et al. [29] who developed a one dimensional model based on simultaneous solutions of continuity equations for charged and excited particles to obtain spatio-temporal distribution for plasma. We note that the fluid transport processes have characteristic velocity scales of the order of $10\text{--}300\text{ ms}^{-1}$ while the velocity scales of the charged species, e.g., the electron velocities are of the order of $10^5\text{ to }10^6\text{ ms}^{-1}$ [30]. Such scale separation allows one to treat the plasma dynamics independently of the fluid dynamics. However, the effects of the plasma dynamics are embedded in the fluid flow conservation equation. The models existing in literature [30–32] provide the plasma generated body force. In Palmeiro and Lavoie [33], a comparative analysis of single dielectric barrier discharge (DBD) was performed and the authors noted that the hybrid model of Lemire and Vo [31] predicted the appropriate trend of the body force quite adequately as compared to other models. It was found to be the only model which exhibited the correct nonlinear velocity scaling with voltage. In this reference the authors have reported experimental measurements of maximum induced velocity in Table 2, for different plasma set-up configurations in quiescent air condition. These measurements show the plasma induced velocity near the electrode (also termed as the ionic wind) is in the range of 1.5 to 2 m/s for the supply voltage of 10 kV with 3 kHz frequency. Such induced velocity near the wing surface would be adequate to mitigate separation and delay transition. This is the motivation of the present study.

A typical schematic of a plasma actuated aerofoil has been shown in Fig. 1 and detailed schematics are shown in Fig. 2, for the associated electrodynamic problem solved near the actuator in different models. Plasma actuators consist of two electrodes separated by insulation (dielectric) covering the lower electrode completely, while the upper one is exposed to the flow, as shown in Fig. 1. In Fig. 2, the computational domain and various governing equations solved for the electrodynamic field are also shown.

In [24, 34–36], experimental results pertaining to plasma control of external flows are reported. In Seraudie et al. [36], a DBD plasma actuator was placed near the leading edge of a modified ONERA-D wing section. According to the authors, the boundary layer was stabilized and was additionally verified by the empirical e^N method using linear stability theory. Incidentally the so called TS wave frequencies for a mean flow of 7 m/s, 10 m/s and 12 m/s were noted to have frequency close to 400 Hz, 600 Hz and 700 Hz, respectively. Increase in flow velocity caused a decrease in turbulent intensity in the tunnel. However, how increase in flow velocity augments the unstable TS wave frequency is not apparent. The authors also note that increase of mean velocity makes the flow less amenable to control by plasma actuation. In contrast, Hanson et al. [34, 35] created experimentally the transition process by a transient growth and not by TS waves, for a Blasius boundary layer. In these experiments, bypass transition was created via the placement of cylindrical roughness elements and the resultant flow was controlled by the plasma actuator. In Kotsonis et al. [24], body force models are provided as a function of voltage and compared with experiments. The authors noted that applied 8 kV (peak to peak) voltage to the electrodes was the onset value for creating an effective plasma. It was also noted that increasing the peak to peak voltage above 16 kV did not alter the plasma anymore. We note here that the required voltage across the electrodes is a strong function of gap between the electrodes. For ex. in [32], a voltage source of 5 kV with 5 kHz frequency was used to study flow separation control in a low pressure turbine cascade when the gap between the electrode was 0.127 mm. In the present work, we have used similar gap between the electrodes with identical voltage ratings.

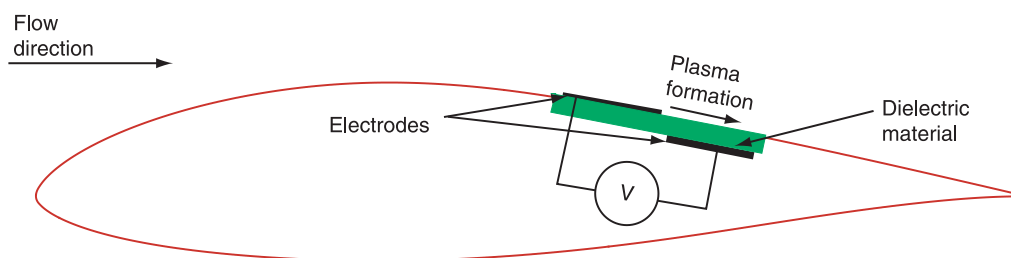


Figure 1. Schematic of a plasma actuator mounted on top surface of DU96-W-180 aerofoil.

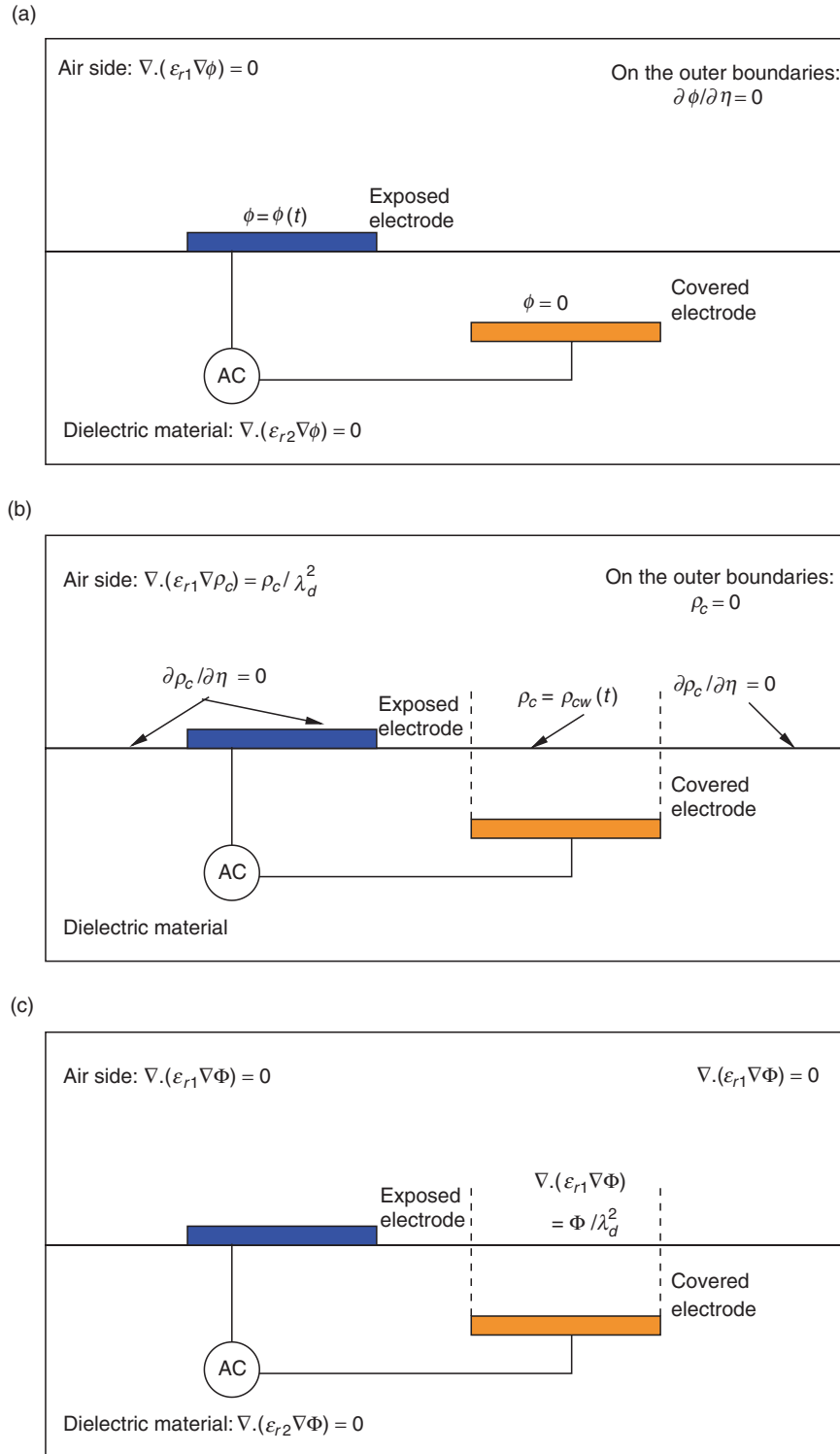


Figure 2. Schematic diagram showing computational domains and boundary conditions for solving (a) eqn. (5); (b) eqn. (7) for a model proposed in [32] and (c) eqn. (8) for a model proposed in [30].

The present paper is formatted in the following manner. Governing equations for plasma are provided in the next section. Governing equations for the fluid dynamical system acted upon by the Lorentz forces are described in section 3. Results and discussions follow in section 4. In section 5, summary and conclusions of the present work are provided.

2. GOVERNING EQUATIONS FOR PLASMA

In case of plasma actuator on the aerofoil, typically a high voltage source is connected to two different electrodes which are separated by a dielectric material, as shown in Fig. 1. One electrode is kept on the surface of the aerofoil while the other electrode is embedded in the surface below the dielectric material. Due to a high voltage difference between two electrodes, air in the vicinity of the electrodes gets weakly ionized. Presence of electric field, exerts a body-force on the flow-field through momentum transfer which can be modeled and incorporated in Navier-Stokes equation.

In a fluid dynamic system excited by plasma actuation, three different time scales exist [30]. The charge distribution occurring in the plasma has the shortest time scale ($\sim 10^{-8}$ sec). The next time scale is present at the level of actuation time required for the plasma actuator which is ($\sim 10^{-4}$ sec). Finally, the third time scale ($\sim 10^{-2}$ sec) is associated with different fluid flow structures. As the first two time scales are very small compared to the actual flow dynamics time scale, one can assume that the charge formation and distribution are almost instantaneous and plasma formation process can be approximated as a quasi-steady process [30]. This assumption forms a basis for adopting equations of electrostatics for describing discharges. A set of Maxwell's equations is used as governing equations to model plasma dynamics. The electro-hydrodynamic force can be expressed as [32]

$$\vec{f}_B = \rho_c \vec{E} + \vec{J} \times \vec{B} \quad (1)$$

As plasma formation and charge redistribution processes are assumed to be instantaneous, following electrostatics equations are adopted. Electric field (\vec{E}) can be derived from the gradient of a scalar potential (Φ) as [32],

$$\vec{E} = -\nabla\Phi \quad (2)$$

Using Maxwell's equation for charge density (ρ_c) one can write,

$$\nabla \cdot (\epsilon \vec{E}) = \rho_c \quad (3)$$

If ϵ_r is a relative permittivity of the medium and ϵ_0 is a permittivity of free-space then the permittivity of the medium is expressed as $\epsilon = \epsilon_r \epsilon_0$. Using eqns. (2) and (3) we obtain,

$$\nabla \cdot (\epsilon \nabla \Phi) = -\rho_c \quad (4)$$

Next, we discuss three important algebraic models developed by different researchers to model body force experienced due to plasma actuation following eqn. (1). We first discuss Suzen et al.'s model [32] which solves two different equations for potential due to the external field and potential due to the net charge density in the plasma to model the body force using eqn. (1). Next model is Orlov's model [30] and has higher complexity. It assumes the air and dielectric material as a parallel network of resistors and capacitors to calculate the charge build-up on the surface of the dielectric. A spatio-temporal lumped-element circuit model has been proposed to model body force using eqn. (1). Finally, we discuss Lemire and Vo's model [31] which is a combination of above two approaches and is superior to previous two approaches as shown in [33]. We have used Lemire and Vo's model [31] for the present computations. Next, these models are discussed in detail.

2.1. Suzen et al.'s model [32]

In the model proposed by Suzen et al. [32], potential Φ in eqn. (2) is composed of the potential due to external electric field (ϕ) and another part which is contributed by the net charge density in the plasma (φ). Characteristic length for electrostatic shielding in a plasma is denoted by the Debye thickness (λ_d). In Suzen et al.'s model [32], it is assumed that λ_d is small and the charge on the wall is not large, which results in two separate equations for the two potentials given by

$$\nabla \cdot (\epsilon \nabla \phi) = 0 \quad (5)$$

$$\nabla \cdot (\epsilon_r \nabla \varphi) = -\frac{\rho_c}{\epsilon_o} \quad (6)$$

Using the net charge density at any point within the plasma [32] given by $\varphi = (-\rho_c \lambda_d^2)/\epsilon_o$ in the above equation, the equation for charge density is obtained as

$$\nabla \cdot (\epsilon_r \nabla \rho_c) = \frac{\rho_c}{\lambda_d^2} \quad (7)$$

In Fig. 2(a), a schematic of the computational domain along with the boundary conditions for the solution of eqn. (5) is shown. Neumann boundary condition is specified at the outer boundaries of the domain while on the electrodes, a time dependent Dirichlet boundary condition is specified. Schematic of a computational domain along with the boundary conditions used in solving eqn. (7) is shown in Fig. 2(b). Boundary condition for ρ_c is given by $\rho_{c,w}$ whose form is based on an assumption and from empirical data. In Suzen et al.'s model [32], downstream of the exposed electrode and on the embedded electrode, the charge density is prescribed as $\rho_{c,w}(x, t) = \rho_c^{\max} G(x) f(t)$ so that it is synchronized with applied voltage $f(t)$. Here, ρ_c^{\max} is the maximum value of charge density and $G(x)$ is a half Gaussian distribution function chosen to resemble plasma distribution over electrode surface as shown in Fig. 4 of [32]. Figure 7 in [32] describes the procedure to obtain Debye length λ_d and maximum charge density on the wall ρ_c^{\max} . A comparison between the experimental and the numerical results show that $\lambda_d = 0.001$ m and $\rho_c^{\max} = 0.0008$ C/m³ are appropriate choices. Body force can be computed from eqn. (1), after obtaining a solution for eqns. (5) and (7) and used subsequently in the Navier-Stokes equations for studying the discharge effects on the flow.

2.2. Orlov's model [30]

In Orlov's model, the governing equation for the potential Φ is derived again using eqn. (4). Assuming steady state, isothermal plasma gas formation and ignoring the diffusion process, the number density of charged particles (n) in the plasma gas is obtained using the following relation

$$n = n_o \exp\left(\frac{e\Phi}{kT}\right).$$

Here the number density of charged particles in the plasma and number density of molecules which are separated into ions and electrons are given by n_i and n_e , respectively. In the above equation, e is the charge of an electron with k is the Boltzmann constant and T is the gas temperature.

If T_i and T_e denote temperatures of ion and electron species and n_i and n_e are the number densities of ions and electrons, respectively, then the net charge density (ρ_c) is related to the electrostatic potential

Φ by $\rho_c = e(n_i - n_e) \simeq -en_o \left(\frac{e\Phi}{kT_i} + \frac{e\Phi}{kT_e} \right)$. Substituting this in eqn. (4) we obtain

$$\nabla \cdot (\epsilon_r \nabla \Phi) = \frac{\Phi}{\lambda_d^2} \quad (8)$$

where the Debye length is defined approximately as 0.00017 m and the charge density is of the order of 10^{16} particles/m³ for plasma generated in ambient pressure [37]. One can define λ_d as

$$\lambda_d = \left[\frac{e^2 n_o}{\epsilon_o} \left(\frac{1}{kT_i} + \frac{1}{kT_e} \right) \right]^{-\frac{1}{2}}.$$

Equation (8) is solved in the domain, as shown in Fig. 2(c). Potential on the electrodes is given by the applied AC voltage: $\Phi|_{electrodes} = \pm\Phi_o$, while on the outer boundaries, the electric potential Φ is set to 0. Electric field \vec{E} given in eqn. (2) can be obtained from the solution of eqn. (8). Body force per unit

volume can be determined from eqn. (1) with magnetic field neglected ($\vec{B} \equiv 0$) using the relation $\rho_c = -\frac{\epsilon_o}{\lambda_d^2} \Phi$, as

$$\vec{f}_B = -\left(\frac{\epsilon_o}{\lambda_d^2}\right) \Phi \vec{E}. \tag{9}$$

The results obtained from the electrostatic model do not account for the charge build up on the surface of the dielectric or change in the volume of plasma as a function of the input voltage, and thus, the results obtained with this model contradicts all the experimental observations [30]. Therefore, a spatial and spatial-temporal lumped-element circuit models were proposed by Orlov [30] to improve upon the existing electrostatic models.

2.2.1. Spatio-Temporal Lumped-Element Circuit Model

In this model, air and dielectric material are represented as a parallel network of resistors and capacitors to calculate the charge build-up on the surface of the dielectric, as in Fig. 3(a). This model has been developed with an aim to represent the ionization process and predict the body force without any experimental calibration [30]. Each parallel network consists of an air capacitor, a dielectric capacitor and a resistive element, as shown in Fig. 3(b). The Zener diodes in the circuit of Fig. 3(b), set the voltage threshold levels for the ionization to occur. Each circuit element consists of two Zener diodes to represent the ionization process, with one of the diodes active during a part of the applied AC voltage cycle. Resistors in the circuit model the plasma formation and its discharge characteristics.

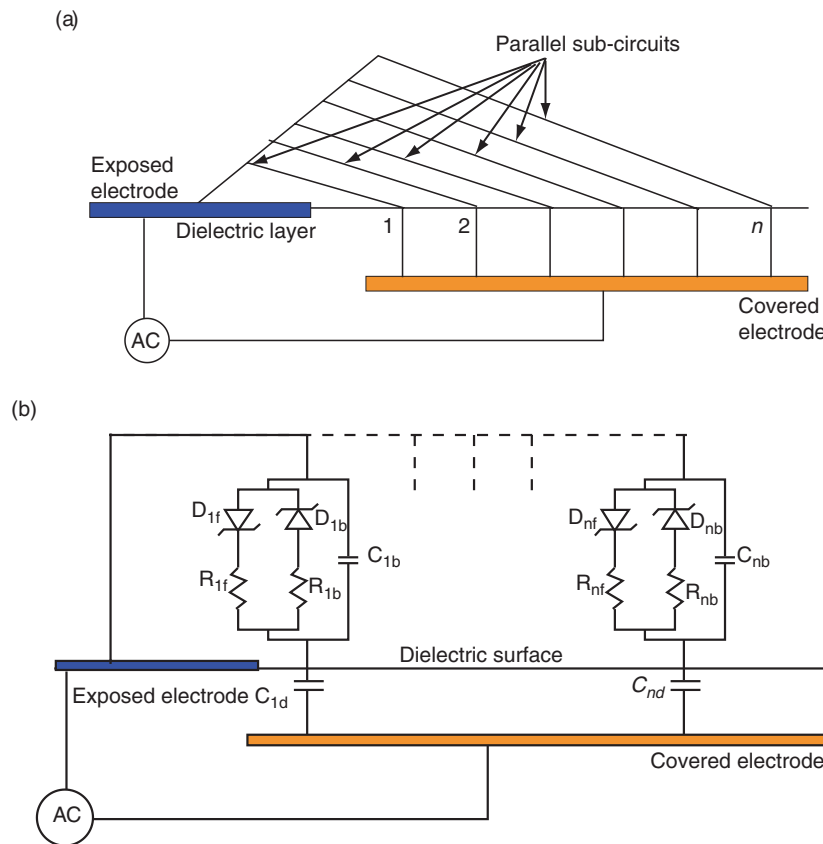


Figure 3. Schematic diagram showing (a) plasma formation region divided into number of parallel sub-circuits and (b) sub-circuit model of a plasma actuator corresponding to the spatio-temporal model of Orlov [30].

Consider ϵ_a as the relative permittivity of air, l_n as the representative distance over the dielectric surface and A_n as a cross-sectional area of the capacitor, which is the product of spanwise size of the actuator (z_n) and the height of the capacitive element (h_n). For the n^{th} sub-circuit, if one denotes ρ_a as the effective resistivity of air, then the value of the air capacitor C_{na} and plasma resistance R_n in the n^{th} sub-circuit is given by

$$C_{na} = \frac{\epsilon_0 \epsilon_a A_n}{l_n} \quad (10)$$

$$R_n = \frac{\rho_a l_n}{A_n}. \quad (11)$$

Similarly the value of the dielectric capacitor for the sub-circuit is given by

$$C_{nd} = \frac{\epsilon_0 \epsilon_d A_d}{l_d} \quad (12)$$

where ϵ_d is the relative permittivity of the dielectric medium, l_d is the thickness of the dielectric material and A_d is the cross-sectional area, which is equal to the product of (z_n) and the width (d_n) of the dielectric capacitor. We observe that all the circuit elements are functions of their distances from the exposed electrode. Based on the actuator geometry and the properties of the materials used, one can evaluate the numerical values of the circuit elements. We can also infer from eqns. (10)–(12) that the farthest sub-circuits have lower air capacitance and larger air resistance. This is in accordance with the physical nature of the problem, where plasma formation is restricted in the vicinity of the two electrodes, due to rapidly decreasing electric field strength away from the electrode. Thus, the effects of plasma are also going to be very localized, allowing a stricter control of the flow.

The voltage on the surface of the dielectric for the n^{th} sub-circuit is determined from

$$\frac{dV_n(t)}{dt} = \frac{dV_{app}(t)}{dt} \left(\frac{C_{na}}{C_{na} + C_{nd}} \right) + k_n \frac{I_{pn}(t)}{C_{na} + C_{nd}}. \quad (13)$$

Here, the applied AC voltage is denoted as V_{app} ; k_n depends on the state of the Zener diode (with $k_n = 1$, when plasma forms, otherwise $k_n = 0$); I_{pn} is the current carried through the plasma resistor. This is an initial value problem, which can be solved numerically using standard solvers. In the following, a detailed description of the algorithm to calculate the applied body force is given.

2.2.2. Algorithm for Calculating Body Force

The following algorithm describes the solution procedure adopted for the body force calculations.

- Determine the circuit parameters and solve the sub-circuit equations for the applied voltage on the dielectric surface, above the embedded electrode. This gives the value of the potential field (Φ) on the surface.
- Use the above values of potential as the Dirichlet boundary condition to solve eqn. (8) with the Debye length specified. The Debye length is chosen based on experimental results and usually is of the order of 0.0001 m. The time dependent potential (Φ) as the boundary condition, incorporates the space-time variation of the plasma.
- Calculate the electric field (\vec{E}) as described earlier and compute the body force using eqn. (9).

The body force thus obtained is incorporated into the Navier-Stokes equation for simulating the effects of plasma on the flow.

2.3. Lemire-Vo's model [31]

A hybrid model [31] combining the features of Suzen et al.'s [32] and Orlov's models [30] was proposed by Lemire & Vo [31], which gives a spatial body force distribution resembling that obtained by more elaborate models used in Gaitonde and co-authors [38, 39]. Here, eqns. (5), (7) are adopted in solving for Φ and ρ_c , during each time step. The boundary conditions over the dielectric layer above the covered electrode $V_n(t)$ and the current $I_{pn}(t)$ are obtained from the spatial-temporal circuit model for the n^{th} element of the parallel circuit model used by Orlov. Voltage distribution on the dielectric surface over the covered electrode ($\Phi = V_n(t)$) thus obtained is used as one of the boundary conditions in solving eqn. (5). This reproduces the physical nature of the output of the plasma actuator which is noted to arrange charges in such a way, so as to annul the applied external electric field [40], as much as possible. This also allows us to define the extent of the plasma created over the dielectric surface. This extent is known to depend on the breakdown voltage gradient of air [31] as modeled by the Zener diode. In the Orlov's model, $V_n(t)$ and $I_{pn}(t)$ are obtained from the amplitude and frequency of the input voltage source.

In Suzen's model, the charge density distribution on the dielectric surface over the covered electrode ($\rho_{cw}(t)$) is specified empirically. In this model [31], it is computed from the current distribution ($I_{pn}(t)$) obtained by the Orlov's model, providing it on the surface by

$$\rho_{cw}(t) = \frac{I_{pn}(t) \times \Delta t}{\text{Volume}} \quad (14)$$

where the denominator represents the volume of the n^{th} electric sub-circuit and Δt corresponds to the time step increment used in computing $V_n(t)$ and $I_{pn}(t)$ by solving eqn. (13). Thereafter, the body force is obtained from $\vec{f}_B = -\rho_c \nabla \Phi$.

3. GOVERNING FLUID DYNAMIC EQUATIONS

We have obtained numerical solution of Navier-Stokes equation using stream function (ψ) - vorticity (ω) formulation. This formulation ensures solenoidality of velocity and vorticity field simultaneously. The (ψ, ω)-formulation is more accurate, as compared to other formulations due to exact satisfaction of mass conservation everywhere. Additionally, we employ an orthogonal grid for the studied incompressible flow which also allows explicit use of orthogonal formulation, resulting in fewer numerical computations per time step and lower numerical errors by discretizing fewer terms with high accuracy schemes for discretization. The resultant accurate numerical solution follows the physical nature of the flow. This latter aspect is best demonstrated by the isotropic treatment of the diffusion operators in orthogonal formulation, as compared to non-orthogonal formulations. The governing Navier-Stokes equation is decoupled into kinematics and kinetics of the flow in the (ψ, ω)-formulation and expressed in an orthogonal grid by the following equations

$$h_1 h_2 \frac{\partial \omega}{\partial t} + h_2 u \frac{\partial \omega}{\partial \xi} + h_1 v \frac{\partial \omega}{\partial \eta} = \frac{1}{\text{Re}} \left[\frac{\partial}{\partial \xi} \left(\frac{h_2}{h_1} \frac{\partial \omega}{\partial \xi} \right) + \frac{\partial}{\partial \eta} \left(\frac{h_1}{h_2} \frac{\partial \omega}{\partial \eta} \right) \right] + \frac{\partial(h_2 F_2)}{\partial \xi} - \frac{\partial(h_1 F_1)}{\partial \eta} \quad (15)$$

$$\frac{\partial}{\partial \xi} \left[\frac{h_2}{h_1} \frac{\partial \psi}{\partial \xi} \right] + \frac{\partial}{\partial \eta} \left[\frac{h_1}{h_2} \frac{\partial \psi}{\partial \eta} \right] = -h_1 h_2 \omega \quad (16)$$

where h_1 and h_2 are the scale factors used in mapping physical (x, y)-plane to a computational (ξ, η)-plane [41], where ξ co-ordinate is in azimuthal direction and η is normal to it. One can define the scale factors by, $h_1 = \sqrt{x_\xi^2 + y_\xi^2}$ and $h_2 = \sqrt{x_\eta^2 + y_\eta^2}$. Plasma actuation causes the body \vec{f}_B force with components given as (F_1, F_2).

For the present computation, we have used an impulsive start, which requires prescribing the irrotational flow as the initial solution. Following boundary conditions are used in solving the governing equations. On the aerofoil surface, no-slip conditions given below are used

$$\psi = \text{constant}; \quad \frac{\partial \psi}{\partial \eta} = 0. \quad (17)$$

These conditions also help fix the wall vorticity, which is required as the boundary condition for the vorticity transport equation, eqn. (15). From the stream function equation, the wall vorticity is calculated as

$$\omega|_{body} = -\frac{1}{h_2^2} \frac{\partial^2 \psi}{\partial \eta^2} \Big|_{body}. \quad (18)$$

In O-grid topology, one introduces a cut starting from the leading edge of the aerofoil to the outer boundary. Periodic boundary conditions apply at the cut, which are introduced to make the computational domain simply-connected. For the stream function equation (eqn. (16)), Sommerfeld boundary condition is used on the η -component of the velocity field at the outer boundary. Resultant value of streamfunction is used to calculate the vorticity value at the outer boundary.

We have used the high accuracy compact scheme SOUCS3 [42] to discretize the convection terms in eqn. (15). This scheme has higher spectral resolution as compared to conventional explicit schemes. For time advancement of the solution, we have used an optimized dispersion relation preserving (DRP) Runge-Kutta scheme OCRK3 - developed in [43]. For discretizing eqn. (16) and the diffusion terms of the vorticity transport equation, we have used second order central differencing scheme. Use of high resolution, neutrally stable DRP scheme ensures a highly space-time accurate numerical solution for the present convection dominated flow.

4. RESULTS AND DISCUSSIONS

In the present work, we have considered a DU96-W-180 aerofoil used for wind turbine applications [44], which is 18% thick. An uniform flow past this airfoil at zero angle of attack (AOA) is considered such that the flow Reynolds number is 4.0×10^5 based on chord (c). An orthogonal grid has been numerically generated with 4972 points in the azimuthal direction and 945 points in the wall normal direction. The first point in the wall normal direction is located at a distance of $10^{-5}c$ from the surface of the aerofoil. A time step of 1.5×10^{-5} is used while solving vorticity transport equation eqn. (15).

In the absence of plasma actuation, this flow has a tendency to form unsteady, small convecting vortices from $x/c = 0.54$ onwards. This is the bypass transition event in the context of enhanced drag experienced by a streamlined body. Having located the onset point of bypass transition, a plasma actuator is located on the surface of the aerofoil with the essential purpose of delaying transition. The plasma actuator is set to work with a potential difference of 5 kV between the electrodes and with a frequency of 5 kHz. Length of the electrodes in the streamwise direction is $0.005c$, while the thickness of the electrodes is around $7 \times 10^{-5}c$. Thickness of the dielectric material in between the electrodes is of the order of $10^{-4}c$. One notes that the actuation frequency is far above the unstable frequencies of TS waves for such varying pressure gradient flows. The effect of actuation at such large frequencies is primarily to cause a steady streaming, which alters the stresses created by the imposed disturbance field, in the opposite way by which Reynolds stresses alters the mean of a turbulent flow. It is also noted that the present simulation is for the time accurate flow field, as opposed to various simulation results presented for time-averaged flows in [22, 23]. Thus, in the present study we show the time accurate flow evolution, with and without the plasma actuation - an exercise not reported before.

Due to plasma actuation, the flow experiences a body force which is evaluated using eqn. (1). In this model, the electrostatic equations are solved at each time step and the corresponding body force evaluated is incorporated for solving the Navier-Stokes equation. Variations of body force per unit volume very near to the exposed electrode, at different instants, are shown in Fig. 4 only for the top

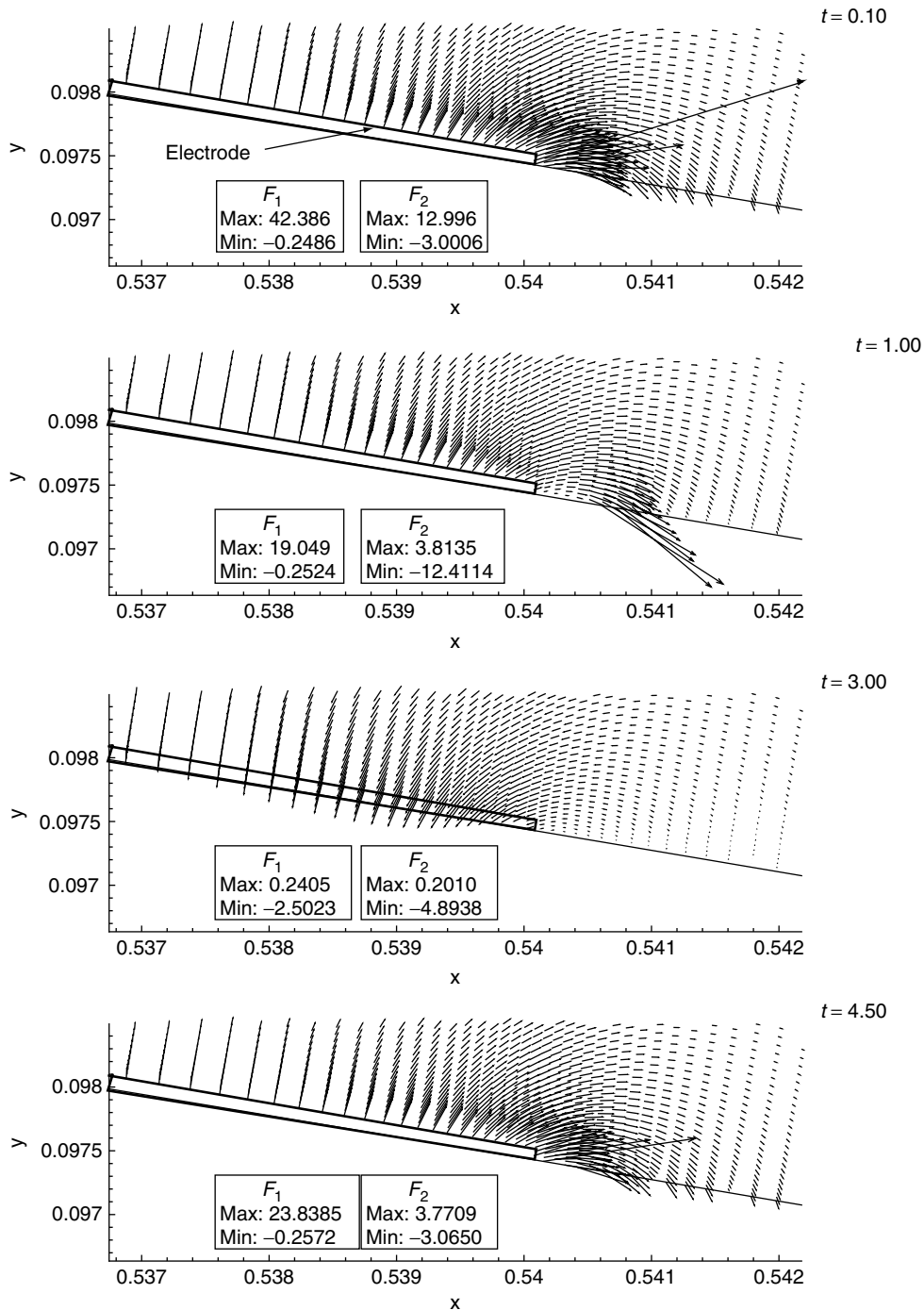


Figure 4. Instantaneous variation of body force vectors (F_1 , F_2) near the electrode on the surface of the aerofoil. Note the maximum and minimum values of (F_1 , F_2) provided at corresponding time.

surface. In this figure, the maximum and the minimum components of the body force are indicated in all the frames. A positive value of F_1 indicates a force component in the downstream direction. Similarly, a negative value of F_2 indicates the force component to be towards the aerofoil. One can observe the localized nature of the body force distribution, with the maximum noted in the gap between the electrodes and which progressively diminishes to a negligible value away from the electrodes. At time $t = 0.10$, one observes a large force vector in the streamwise direction near the tip of the electrode. The overall body force distribution is in the streamwise direction which helps

to delay flow transition due to adverse pressure gradient near the trailing edge. Such body force distribution is also seen at $t = 1.0$ and 4.5 . At $t = 3.0$, the force vectors are directed towards the surface causing reduction of boundary layer thickness in adverse pressure gradient region, which is otherwise seen to cause wall normal vortical eruptions during bypass transition. Thus the plasma actuation assists the flow on the aerofoil to remain laminar by suppressing events during bypass transition.

We have shown the effects of plasma actuation on top surface of the aerofoil at different streamwise locations and at different times. In Fig. 5(a), we have shown the variation of streamwise

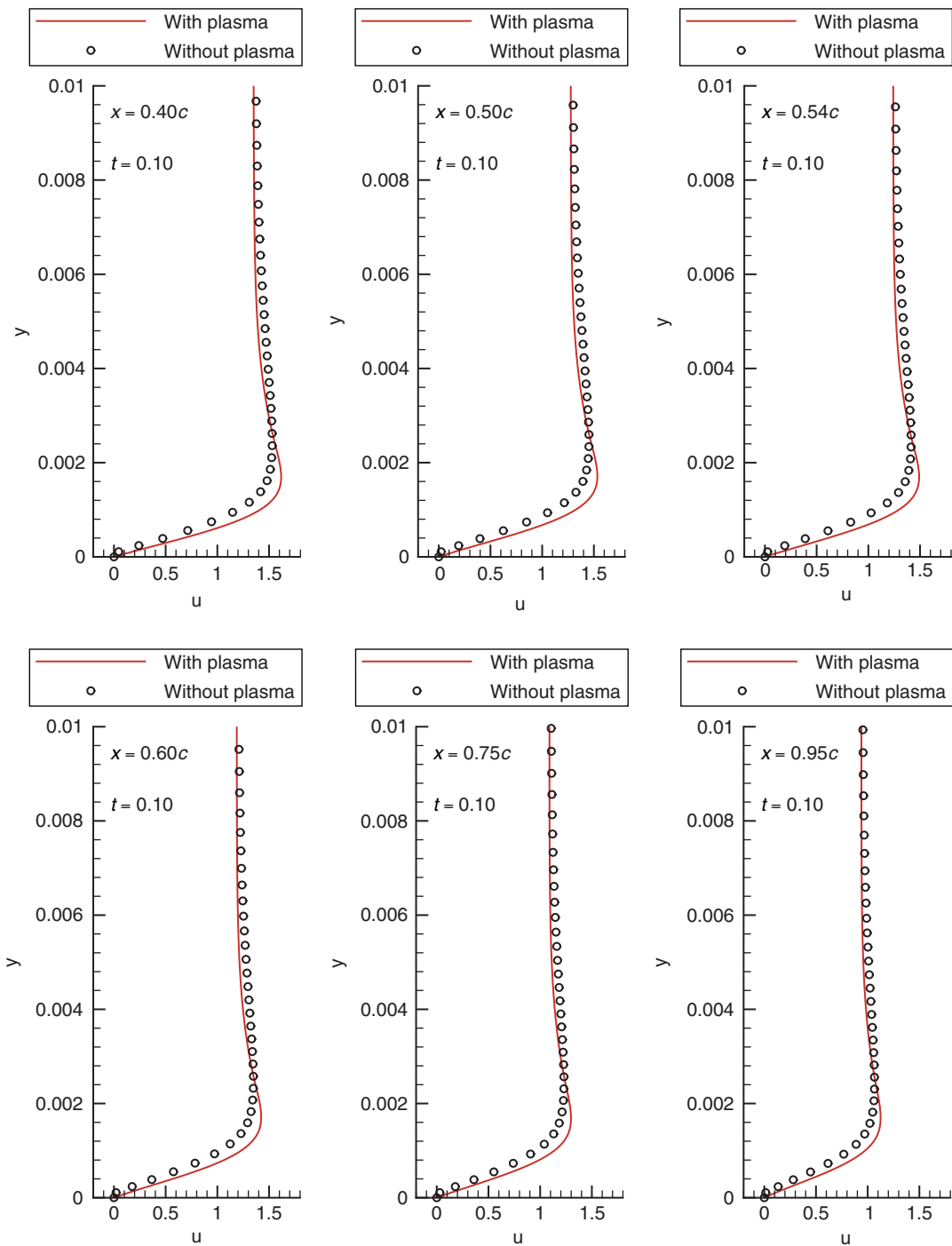


Figure 5(a). Variation of azimuthal component of the velocity with and without plasma actuation at different locations on top surface of the aerofoil at $t = 0.10$.

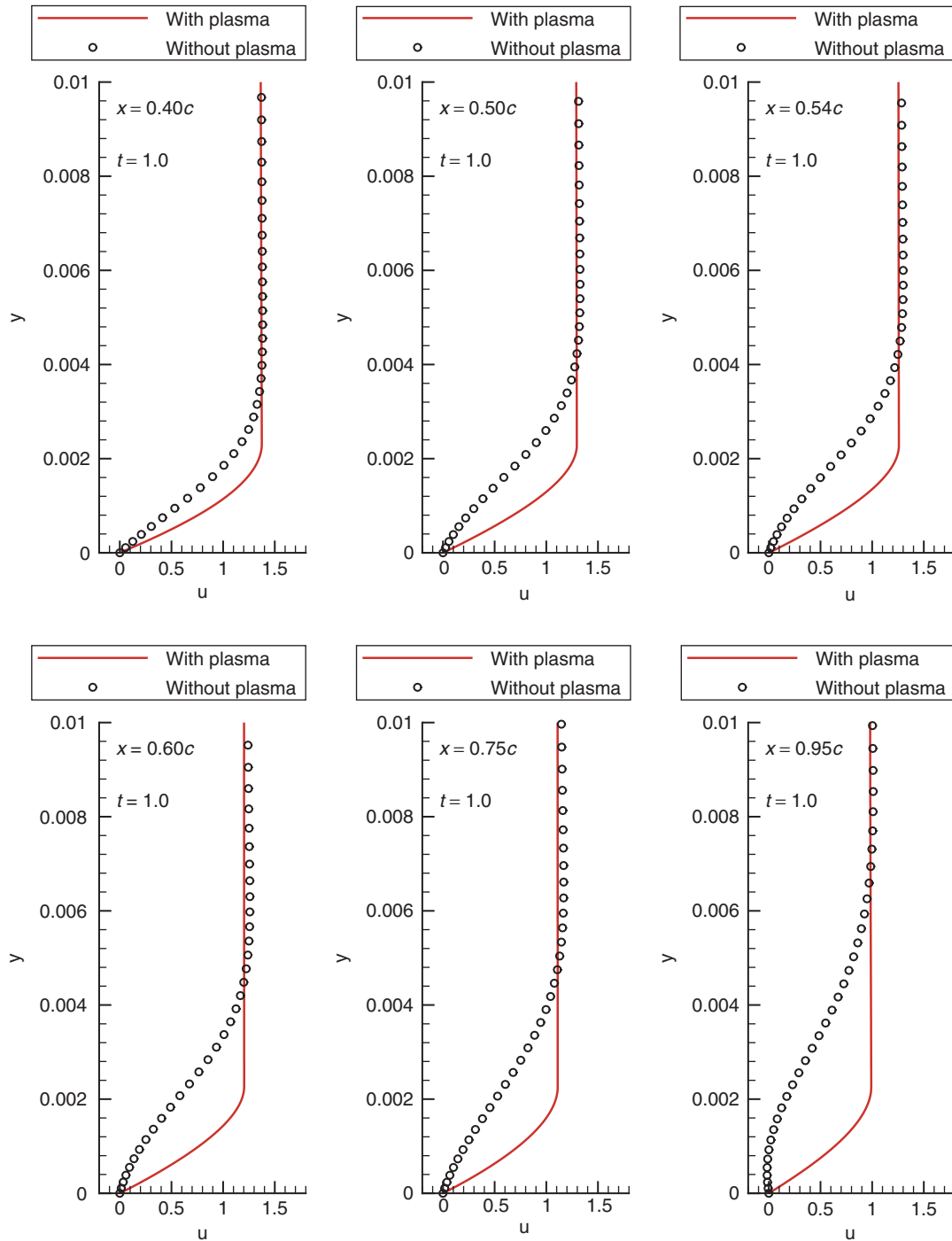


Figure 5(b). Variation of azimuthal component of the velocity with and without plasma actuation at different locations on top surface of the aerofoil at $t = 1.00$.

velocity component at $t = 0.10$, with and without the plasma actuation for different streamwise locations. One can observe that with plasma actuation, the flow has fuller streamwise velocity profiles in the boundary layer region as compared to the no actuation case. Maximum value of streamwise component of the velocity also decreases as one moves from $x = 0.40c$ to $x = 0.95c$, due to adverse pressure gradient. However, at this early time, one does not observe any presence of smallscale unsteady separation bubbles in the actuated and non-actuated cases, whose presence would have been evident from localized reverse flow velocity profile. In Fig. 5(b) at $t = 1.0$, for the

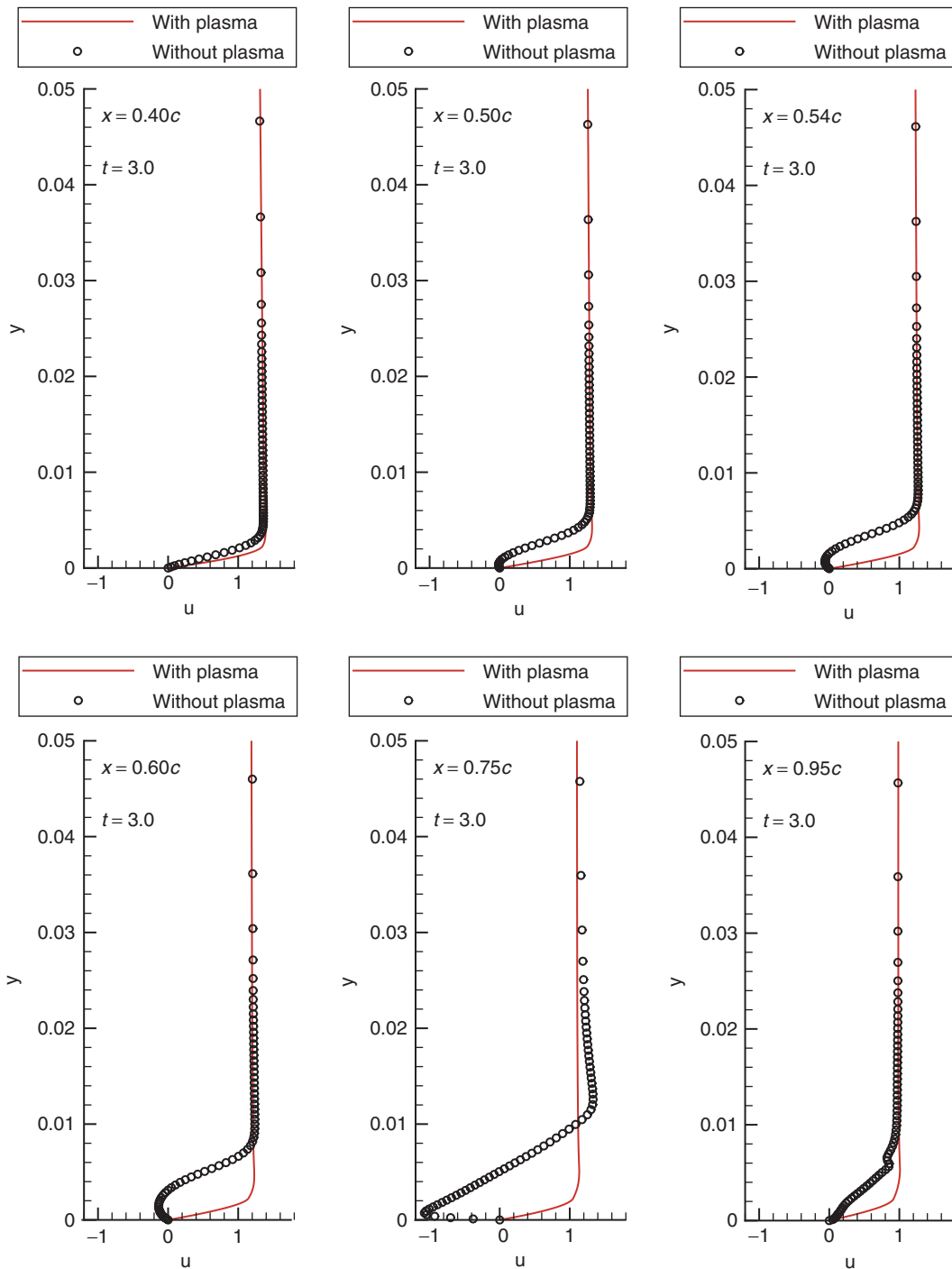


Figure 5(c). Variation of azimuthal component of the velocity with and without plasma actuation at different locations on top surface of the aerofoil at $t = 3.00$.

case of no plasma actuation, one notices the growth of boundary layer in the wall normal direction, which is highest at $x = 0.95c$ for the compared velocity profiles. This is due to a strong adverse pressure gradient region near the trailing edge, with the flow showing higher tendency to form separation bubbles. In contrast, for the case with plasma actuation, one does not note any large growth of the boundary layer. In Fig. 5(c) for the flow at $t = 3.0$, velocity profiles corresponding to no actuation cases show flow separation after $x = 0.54c$ onwards, while for the case with plasma actuation, flow retardation caused by adverse pressure gradient is not seen, with the velocity

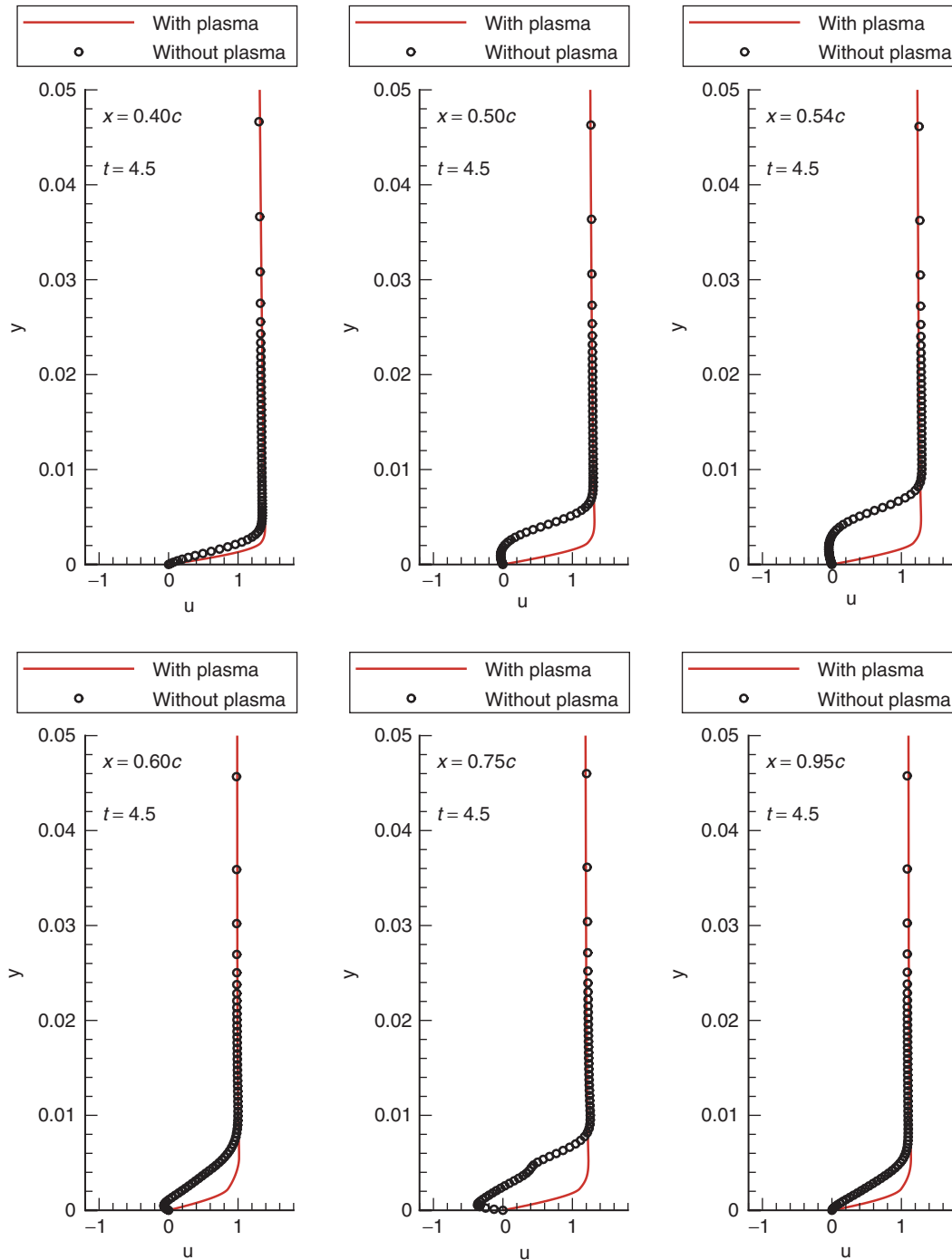


Figure 5(d). Variation of azimuthal component of the velocity with and without plasma actuation at different locations on top surface of the aerofoil at $t = 4.50$.

profiles significantly fuller - an indication of favourable pressure gradient caused by plasma actuation. This observation is also seen at the later time of $t = 4.50$ in Fig. 5(d) - implying the continual stabilizing tendency of plasma actuation.

In Fig. 6, we have shown variation of vorticity at different instants on the top surface of the aerofoil, with and without plasma actuation. For the case of no actuation, one notices large wall vorticity gradients due to bypass transition causing unsteady separations. However, at the early time of $t = 0.10$, one cannot observe presence of such large vorticity gradients, for both the cases. This also happens to be the case at $t = 1.0$, where large gradients are not noted for either cases. Instead for the case of plasma actuation, one notices low wavenumber variation of wall vorticity which does not

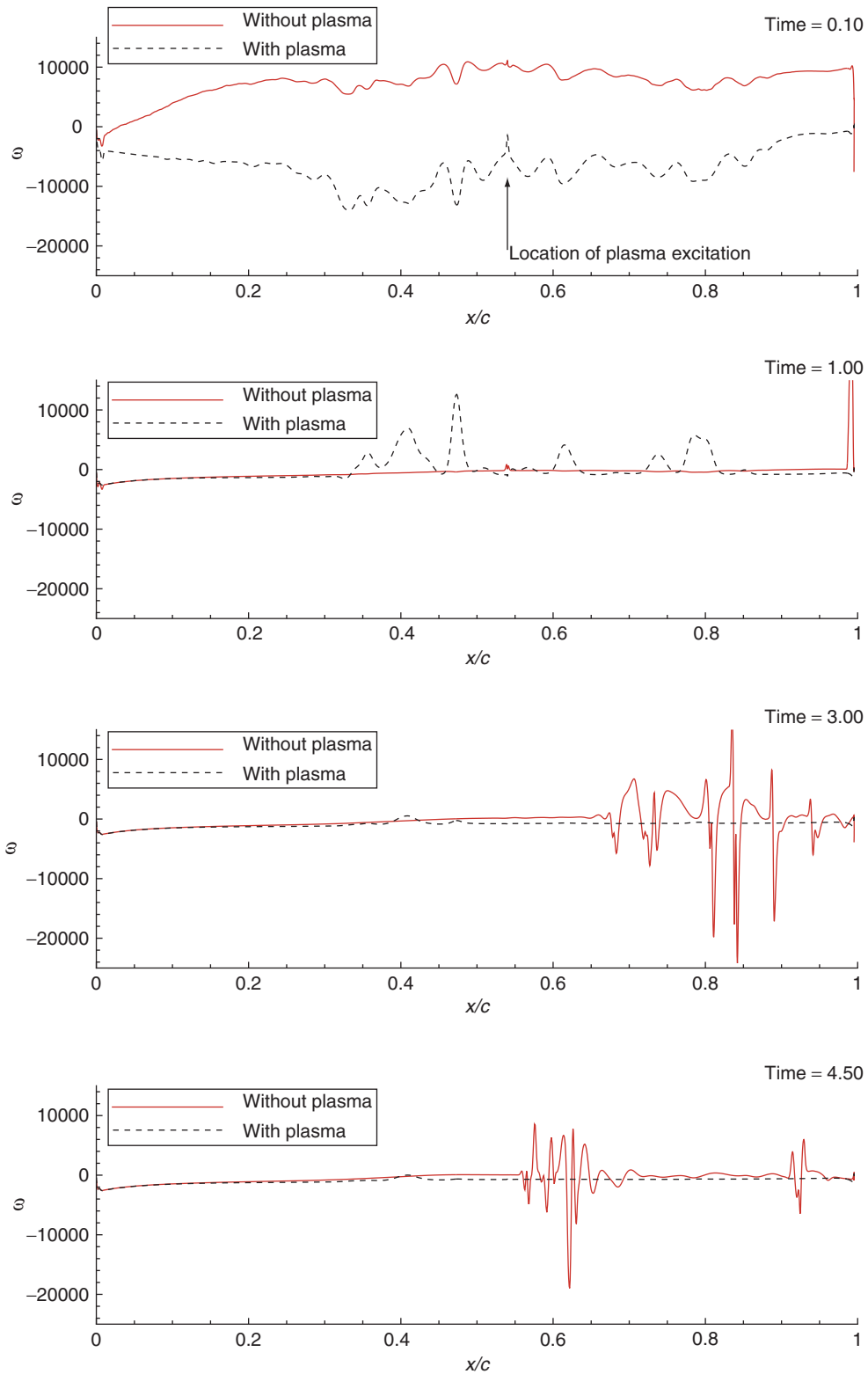


Figure 6. Variation of surface vorticity on top surface of the aerofoil with and without plasma actuation at different instants.

trigger any separation. Presence of large vorticity disturbances for the no plasma actuation case are observed at $t = 3.0$ and 4.50 in Fig. 6. For the case with plasma actuation, such unsteady separations have been suppressed at the later instances.

5. SUMMARY AND CONCLUSIONS

In the present work, we have studied the control of flow by plasma actuation, over a DU96-W-180 aerofoil at zero AOA for $Re = 4.0 \times 10^5$. In order to model the plasma formation and its contribution to generate a body force term needed to be incorporated in Navier-Stokes equation, we have used a hybrid model of Lemire and Vo [31]. In this model, along with the numerical simulation of Navier-Stokes equation, at each time step one solves eqns. (5) and (7) for the body force. The boundary conditions for $V_n(t)$ and $I_{pn}(t)$ over the dielectric layer above the covered electrode are obtained from the spatio-temporal circuit model used by Orlov [30].

We have shown schematic of a plasma actuator mounted on the aerofoil surface in Fig. 1, while Fig. 2 shows schematics of computational domains and corresponding boundary conditions for the plasma simulation models of Suzen et al. [32] and Orlov [30]. Schematic of circuit model of a plasma actuator corresponding to spatio-temporal lumped-element circuit model of Orlov is shown in Fig. 3. Variation of instantaneous body force vectors at different instants near the exposed electrode on the surface of the aerofoil has been shown in Fig. 4. In this figure, one can observe the direction of the body force to be in the streamwise direction, which can stabilize the flow by plasma actuation. Due to the action of plasma, the body force induces an ionic wind which can change the velocity profile favourably, where the flow has the tendency to recirculate otherwise. This has been shown at different times in Figs. 5(a)–5(d). Comparison of velocity profiles at different stations on aerofoil surface shows that the case with plasma actuation does not show any localized flow reversal (signature of bypass transition) while the non actuated case shows velocity profiles with flow reversal beyond $x = 0.54c$. This is also evident from Fig. 6, in which vorticity variations on the top surface of the aerofoil are shown, for the cases with and without plasma actuation. Without plasma actuation, formation of steep vorticity gradient which leads to unsteady flow separation beyond mid-chord of the aerofoil is noted, while such disturbances are absent for the case with plasma actuation with 5 kV applied voltage between the electrodes at 5 kHz frequency.

In future, the scope of this calculation will be enhanced by studying other cases for different airfoils with different parameters of plasma actuation.

REFERENCES

- [1] Sengupta, T.K. and Poinso T., *Instabilities of Flows: With and Without Heat Transfer and Chemical Reaction*, Springer Wien, New York, 2010.
- [2] Morkovin, M.V., *On the many faces of transition*, Wells CS, editor. Viscous Drag Reduction 1–31, Plenum Press, New York, 1969.
- [3] Bhumkar, Y.G., *High Performance Computing of Bypass Transition*, Ph.D. Thesis, IIT Kanpur, 2012.
- [4] Sengupta, T.K. and Bhaumik, S., Onset of turbulence from the receptivity stage of fluid flows, *Physical Review: Letters*, 2011, 107, 154501.
- [5] Velkoff, H. and Ketcham, J., Effect of an electrostatic field on boundary-layer transition, *AIAA*, 1968, 6(7), 1381–1383.
- [6] Corke, T.C. and Post, M.L., Overview of plasma flow control: concepts, optimization and applications, *43rd AIAA Aerospace Sciences Meeting and Exhibit* (Reno, NV), AIAA Paper, 2005, 2005-563.
- [7] Corke, T.C., Jumper, E.J., Post, M.L., Orlov, D.M., and McLaughlin, T.E., Application of weakly-ionized plasmas as wing flow-control devices, *AIAA Paper*, 2002, 2002–0350.
- [8] Patel, M.P., Sowle, Z.H., Corke, T.C. and He, C., Autonomous Sensing and Control of Wing Stall Using a Smart Plasma Slat, *Journal of Aircraft*, 2007, 44, 516–527.
- [9] Huang, J., Corke, T.C. and Thomas, F.O., Plasma actuators for separation control of low pressure turbine blades, *AIAA Paper*, 2003, 2003–1027.
- [10] List, J., Byerley, A.R., McLaughlin, T.E. and VanDyken, R.D., Using a plasma actuator to control laminar separation on a linear cascade turbine blade, *AIAA Paper*, 2003, 2003–1026.
- [11] Asghar, A., Jumper, E.J. and Corke, T.C., On the use of Reynolds number as the scaling parameter for the performance of plasma actuator in a weakly compressible flow, *AIAA Paper*, 2006, 2006–21.
- [12] Thomas, F.O., Kozlov, A. and Corke, T.C., Plasma actuators for bluff body flow control, *AIAA Paper*, 2006, 2006–2845.

- [13] Hultgren, L.S. and Ashpis, D.E., Demonstration of separation delay with glow-discharge plasma actuators, AIAA Paper, 2003, 2003–1025.
- [14] Riherd, M. and Roy, S., Numerical investigation of serpentine plasma actuators for separation control at low Reynolds number, AIAA Paper, 2011, 2011–3990.
- [15] Visbal, M.R. and Gaitonde, D.V., Control of vortical flows using simulated plasma actuators, AIAA Paper, 2006, 2006–505.
- [16] Corke, T.C., He, C. and Patel, M., Plasma flaps and slats: an application of weakly-ionized plasma actuators, AIAA Paper, 2004, 2004–2127.
- [17] Post, M.L. and Corke, T.C., Separation control using plasma actuators-stationary and oscillatory airfoils, AIAA Paper, 2004, 2004–0841.
- [18] Huang, X., Zhang, X. and Li, Y., Broadband flow-induced sound control using plasma actuators, *Journal of Sound and Vibration*, 2010, 329, 2477–2489.
- [19] Wilkinson, S.P., Investigation of an oscillating surface plasma for turbulent drag reduction, AIAA Paper, 2003, 2003–1023.
- [20] Grundmann, S. and Tropea, C., Experimental transition delay using glow-discharge plasma actuators, *Experiments in Fluids*, 2007, 42, 653–657.
- [21] Grundmann, S. and Tropea, C., Active cancellation of artificially introduced Tollmien-Schlichting waves using plasma actuators, *Experiments in Fluids*, 2008, 44, 795–806.
- [22] Cristofolini, A., Neretti, G., Roveda, F. and Boghi, C.A., Experimental and numerical investigation on a DBD actuator for airflow control, AIAA Paper, 2011, 2011–3912.
- [23] Gaitonde, D.V., Visbal, M.R. and Roy, S., Control of flow past a wing section with plasma-based body forces, AIAA Paper, 2005, 2005–5302.
- [24] Kotsonis, M., Giepmans, R. and Veldhuis, L., Numerical study on control of Tollmien-Schlichting waves using plasma actuators, AIAA Paper, 2011, 2011–3175.
- [25] Rizzetta, D.P. and Visbal M.R., Exploration of plasma-based control for low-Reynolds number airfoil/gust interaction, AIAA Paper, 2011, 2011–3252.
- [26] Suman, V.K., *Effects of Plasma Actuation on Flow Past Natural Laminar Flow (SHM-1) Airfoil*, M.Tech. Thesis, IIT Kanpur, 2010.
- [27] Sreejith, N.A., *Effects of Plasma for Transonic Flow Past an Airfoil*, M.Tech. Thesis, IIT Kanpur, 2011.
- [28] Zhang, X., Luo, X. and Chen, P., Airflow control using plasma actuation and Coanda effect, AIAA Paper, 2011, 2011–3516.
- [29] Massines, F., Rabehi, A., Decomps, P., Ben Gadri, R., Segur, P. and Mayoux, C., Experimental and theoretical study of a glow discharge at atmospheric pressure controlled by dielectric barrier, *Journal of Applied Physics*, 1998, 83, 41–52.
- [30] Orlov, D.M., *Modelling and simulation of single dielectric barrier discharge plasma actuators*, Ph.D. Thesis, University of Notre Dame, 2006.
- [31] Lemire, S. and Vo, H.D., Reduction of fan and compressor wake defect using plasma actuation for tonal noise reduction, *Journal of Turbomachinery*, 2011, 133(1), 011017.
- [32] Suzen, Y., Huang, P.G., Jacob, J.D. and Ashpis, D.E., Numerical simulation of plasma based flow control applications, AIAA Paper, 2005, 2005–4633.
- [33] Palmeiro, D. and Lavoie, P., Comparative analysis on single dielectric barrier discharge plasma actuator models, *7th International Symposium on Turbulence and Shear Flow Phenomena, Ottawa, Canada*, 2011.
- [34] Hanson, R.E., Lavoie, P. and Naguib, A.M., Effect of plasma actuator excitation for controlling bypass transition in boundary layers, AIAA Paper, 2010, 2010–1091.
- [35] Hanson, R.E., Lavoie, P., Naguib, A.M. and Morrison, J.F., Transient growth instability cancellation by a plasma actuator array, *Experiments in Fluids*, 2010, 49, 1339–1348.
- [36] Seraudie, S., Vermeersch, O. and Arnal, D., DBD plasma actuator effect on a 2D model laminar boundary layer. Transition delay under ionic wind effect, AIAA Paper, 2011, 2011–3515.
- [37] Roth, J., *Industrial Plasma Engineering: Volume 1: Principles*, Taylor & Francis, CRC Press, 1995.

- [38] Gaitonde, D.V., Visbal, M.R. and Roy, S., A coupled approach for plasma-based flow control simulations of wing sections, AIAA Paper, 2006, 2006–1205.
- [39] Roy, S., Singh, K.P., Haribalan, K., Gaitonde, D.V. and Visbal, M.R., Effective discharge dynamics for plasma actuators, AIAA Paper, 2006, 2006–374.
- [40] Enloe, C.L., McLaughlin, T.E., VanDyken, R.D., Kachner, K.D., Jumper, E.J. and Corke, T.C., Mechanisms and responses of a single dielectric barrier plasma, AIAA Paper, 2003, 2003–1021.
- [41] Sengupta, T.K., *Fundamentals of Computational Fluid Dynamics*, Universities Press, Hyderabad, 2004.
- [42] Dipankar, A. and Sengupta, T.K., Symmetrized compact scheme for receptivity study of 2D transitional channel flow, *Journal of Computational Physics*, 2006, 215, 245–273.
- [43] Sengupta, T.K., Rajpoot, M.K. and Bhumkar, Y.G., Space-time discretizing optimal DRP schemes for flow and wave propagation problems, *Computers and Fluids*, 2011, 47, 144–154.
- [44] Ghosh, S., *Plasma actuation for active control of wind turbine power*, M.Sc. Thesis, Ecole Polytechnique de Montreal, 2012.